Available online at www.sciencedirect.com

SciVerse ScienceDirect

Physics Procedia 36 (2012) 187 – 192

Physics Procedia

Superconductivity Centennial Conference

# Parasitic Losses in Nb Superconducting Resonators

J. M. Hornibrook[a,b], E. E. Mitchell[a], C. J. Lewis[a] and D. J. Reilly[b]

[a]*CSIRO Material Science and Engineering, Lindfield, NSW 2070, Australia*
[b]*ARC Centre of Excellence for Engineered Quantum Systems, School of Physics, The University of Sydney, NSW 2006, Australia*

**Abstract**

Microwave losses in niobium (Nb) superconducting resonators are investigated at milli-Kelvin temperatures and with low drive power. In addition to the well-known suppression in *Q*-factor that arises from coupling between the resonator and two-level defects in the dielectric substrate, we report strong dependence of the measured *Q*-factor and resonance line-shape on the electromagnetic environment. Methods to suppress parasitic coupling between the resonator and its environment are discussed.



*Keywords*: microwave coplanar waveguide; superconducting; two-level systems; quantum information processing

## 1. Introduction

Lithographically-defined superconducting transmission line resonators are key passive circuit elements in the storage and distribution of microwave electromagnetic (EM) fields on-chip. Their very low dissipation, inherent to the superconducting state, opens the prospect of using these integrated devices in the context of parametric amplification [1,2], single photon detection [3], and as a means of transferring quantum information in solid-state technologies [4,5]. Enabling such applications however, requires a detailed understanding of the loss mechanisms that limit the quality (*Q*-) factor of these simple structures, particularly in the low power limit where the resonator is occupied by a single microwave photon at a time.

It is now well established that loss mechanisms in the dielectric material comprising the resonator substrate can limit *Q*-factors at milli-Kelvin temperatures [6-8]. Specifically, two-level electron traps arising from materials defects in the dielectric open a channel for enhanced relaxation or emission of photons from the resonator, dominating loss at low drive power. In addition, the Purcell effect, where the

1875-3892  doi:10.1016/j.phpro.2012.06.069

electromagnetic environment of the resonator influences the rate of spontaneous emission, yields further mechanisms for energy dissipation in these superconducting circuits.

Here we investigate loss mechanisms for niobium coplanar resonators fabricated on magnesium oxide dielectric substrates. Microwave transmission measurements are made at milli-Kelvin temperatures to determine resonator $Q$-factors. Numerical EM simulations are used to guide device design and illustrate the effect of parasitic coupling on the resonator $Q$ and resonance frequency. We compare $Q$-factor measurements for two different sample mounts and discuss the resonance line-shape for these different parasitic EM environments.

## 2. Design and Fabrication

### *2.1. Resonator design*

Our resonators are constructed using a coplanar waveguide architecture. The layout for a half wavelength resonator is shown in Fig. 1, where $w$ = 10 μm is the width of the center conductor and $g$ = 4.6 μm is the gap between the center conductor and the ground planes (light regions are niobium, dark regions are the substrate below). The effective permittivity $\varepsilon_{eff}$ and consequently the characteristic impedance of the transmission line ($Z_o$ = 50 Ω) is set by the geometry (defined by $w$ and $g$) and the substrate dielectric constant $\varepsilon$. Both $Z_o$ and the resonance frequency $f_o$ are determined analytically [9]. Capacitors with values of ~ 0.4 pF are used to couple the resonator to the input and output ports. The resonant frequency is then given by the distance between coupling capacitors, $l$, as $f_0 = c/2l\sqrt{\varepsilon_{eff}}$.

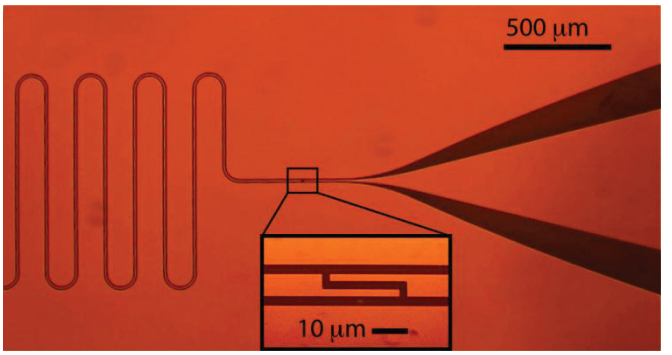


Figure 1: Half wavelength coplanar resonator showing tapered contact pad at right with coupling capacitor shown in zoom. The light areas are the Nb film and the dark areas the substrate between the centre conductor and the ground plane.

### *2.2. Resonator Fabrication*

Resonator devices are fabricated by depositing thin Nb films (150 nm) on magnesium oxide (MgO) substrates using dc magnetron sputtering. To improve the adhesion of thicker Nb films to the substrates (films thicker than ~ 50 nm can lift off the substrate during fabrication), substrates are first cleaned by light ion beam milling (300 V, 10 minutes), with the Nb films subsequently sputtered at 1 × $10^{-7}$ mb without breaking vacuum. Surface roughness of the MgO substrate, characterized using a profilometer, is significantly reduced by the ion beam process. Films deposited under these conditions have a critical current density of $J_c$ ~ 17 MAcm$^{-2}$ and critical temperature $T_c$ ~ 8.8 K. To simplify the resonator structure a final contact layer of gold is avoided since the 2–3 nm niobium surface oxide layer does not impede aluminum wire bonding.

Standard photolithographic techniques are used to pattern the devices, with excess Nb removed via argon ion beam milling. Resonator lengths are typically ~15 mm, with a distance of 180 μm between adjacent meanderings to prevent electromagnetic coupling (see Fig. 1) and resonance frequencies in the range $f_0$ ~ 3–5 GHz. We now turn to examine the resonator performance arising from different contact pad geometries and sample enclosure designs.

### *2.3. Sample enclosure design*

Resonator sample chips are mounted in brass or copper "light-tight" enclosures and thermally anchored to the mixing chamber of a dilution refrigerator (*Leiden Cryogenics Co*). Microwave SMA feed-through connectors mate with semi-rigid coaxial cables that are in thermal contact with the lowest temperature stage of the refrigerator. The geometry of the sample enclosure is designed to have sufficiently small internal dimensions such that the frequency of standing wave modes is well away from the resonator frequency [10].

Two different enclosures are investigated as shown in Fig. 2. The enclosure shown in Fig. 2(a) is a gold-coated brass box. Shallow slots milled in the brass accommodate the MgO substrate (10 mm × 5 mm), with sapphire microstrip waveguides (*US Microwaves Co*) connecting the resonator chip to the SMA connectors. A thin layer of soft electroplated gold enables wire bonding.

A second sample enclosure (Fig. 2(b)) makes use of a printed circuit board (PCB) to connect the sample to the SMA connectors. The PCB is a *Rogers* laminate 6010 allowing the dielectric constant to closely match that of our substrates (MgO: 9.5; Rogers 6010: 10.2), with 1 oz. Cu and a thin layer of wire bondable gold on the top surface. The PCB features a coplanar waveguide with a tapered center conductor to match the SMA connector geometry to the contact pads on the resonator chip. The chip is wire bonded to the PCB using 25 μm diameter wire bonds. We use three wire bonds at each centre conductor and around 100 wire bonds for the grounding. Multiple vias connect ground planes on the top and bottom of the PCB in order to prevent direct parasitic EM coupling between input and output ports.

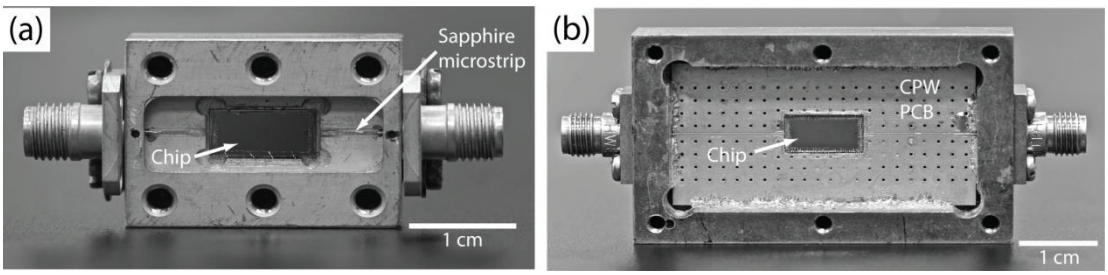


Figure 2: Two different sample enclosures (a) Au-coated box with "field-replaceable" 50 Ω connectors and saphire microstrips and (b) PCB enclosure design with matched dielectric constants for MgO and sapphire.

### *2.4. Microwave Measurement Setup*

Low temperature resonator loss is determined via *S*-parameter measurements, making use of a microwave vector network analyzer (N5230C *Agilent Co,* 8510C *HP Co*). High frequency connections from room temperature to the sample are made using stainless steel and BeCu semi-rigid coaxial cables (UT85 *Microcoax Co*). On the input line, attenuators (*XMA Co*) thermalize the coax center conductor at each temperature stage, giving a total attenuation of ~ 60 dB before the sample. Low pass filters (*Minicircuits Co*) with a 3 dB frequency of 7.6 GHz are used at the 50 mK stage of the refrigerator to

prevent excess high frequency noise from reaching the sample. Transmission measurements are made by following the sample with a cryogenic microwave amplifier mounted at 4 K (noise temperature ~ 3 K, gain ~ 42 dB, LNC4_8A *Low Noise Factory Co*) and additional amplification at room temperature (+24 dB *Miteq Co*). Temperature is determined using a calibrated carbon thermometer anchored to the refrigerator mixing chamber.

## 3. Microwave Transmission Measurements and Simulation Results

### *3.1. Effect of Coplanar Waveguide Design*

Turning to our results we note that previous investigations have considered the effect of coplanar resonator geometry on $Q$-factor. To date, the coplanar width and gap [11], meander layout [12], film thickness [13] and substrate dielectric materials [6] have been considered. Here we investigate how the shape of the on-chip tapered interconnects, between the bond pad and resonator, affects the measured microwave $S$-parameters. Keeping the characteristic impedance constant at 50 Ω, Fig. 3(a) shows the results of numerical simulations (using *Ansoft's HFSS* package) for different tapering geometries.

We contrast the response of smooth tapering in the width and gap of the waveguide, shown in Fig. 3(b), with the more abrupt transition in waveguide geometry shown in Fig. 3(c). The EM simulations show that the abrupt tapering leads to a shift in the resonance to lower frequencies. In addition, a smaller peak in the transmission response is seen to appear. Note that in both tapering geometries the ratio of width and gap distance in the waveguide is chosen to maintain a constant characteristic impedance of 50 Ω. The resonator is sensitive however, to geometric changes close to the boundaries as the evanescent EM wave decays over this length-scale. It is the evanescent decay that yields the sensitivity to the waveguide tapering.

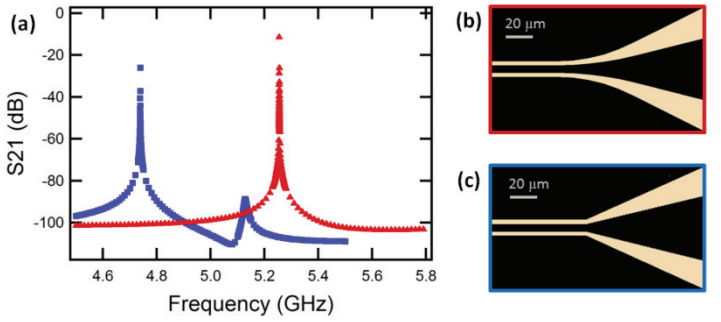


Figure 3: Numerical simulations using *Ansoft's HFSS* package. (a) Numerical results for smooth (red) and abrupt (blue) tapering of the coplanar waveguide connecting the resonator to the bond pad. (b) Schematic of the smooth tapering geometry. (c) Schematic of the abrupt tapering geometry.

### *3.2. Parasitic Environment Line-shape and Q-factor*

As we have shown using simulations, the electromagnetic (or impedance) environment in which the resonator is embedded can impact on the resonator performance, affecting the resonance frequency and measured $Q$-factor. The measured resonator $Q$-factor, $Q_M$, is related to the internal loss $1/Q_{int}$ and external loss $1/Q_{ext}$ via

$$\frac{1}{Q_M} = \frac{1}{Q_{int}} + \frac{1}{Q_{ext}}$$

We now expand on this concept and compare microwave transmission data for two resonators with different EM environments, extracting $Q_M$ in each case. Both resonator samples are fabricated on MgO substrates using the fabrication procedure described above. Where possible, we have attempted to ensure identical conditions to facilitate the comparison between the two samples.

We find that the combination of the sample enclosure shown in Fig. 2(a), the use of microstrip transmission lines connecting the sample, and fewer grounding paths near the geometry transition leads to a resonance response that is asymmetric with respect to frequency, as shown, for instance, in Fig. 4(a). Several such devices were measured in this configuration of EM environment and found to yield similar line-shapes, as well as a distribution in resonance frequencies despite nominally identical fabrication conditions.

Given an asymmetric resonance, we extract $Q$-factors via a fit (red line in Fig. 4(a)) to a modified Lorentzian line-shape for the measured transmission coefficient $S_{21}$ as a function of frequency $f$ [8]:

$$S_{21} = \left| \frac{r}{1 + 2iQ_M (f - f_0)/f_0} + Ae^{i\varphi} \right| \tag{1}$$

where $f_0$ is the resonance frequency, $Q_M$ is the measured $Q$-factor and $r$ a fit parameter that scales the height of the resonance. The term $A\exp(i\phi)$ is also a free parameter of the fit that characterises the non-resonant, parasitic path between input and output ports. Because of the number of free parameters, we stress that this fit is used primarily to qualitatively describe the line-shape of the resonance.

Contrasting the asymmetric response, Fig. 4(b) shows data taken on a resonator in which strong attempts have been made to mitigate parasitic coupling. These include smooth tapering of interconnects, the addition of a large number of grounding bonds between the resonator and sample enclosure, and the use of a PCB that is matched to the effective permittivity of the resonator. We find that this combination reduces parasitic coupling between input and output ports and yields a resonance that is characteristic of a Lorentzian. Reducing the term $A\exp(i\phi)$, in the fit recovers the near Lorentzian lineshape expected when interaction with the non-resonant parasitic path is suppressed (red line in Fig. 4(b)). For devices embedded in this low parasitic EM environment we find that resonator frequencies agree with predicted values within 2 %.

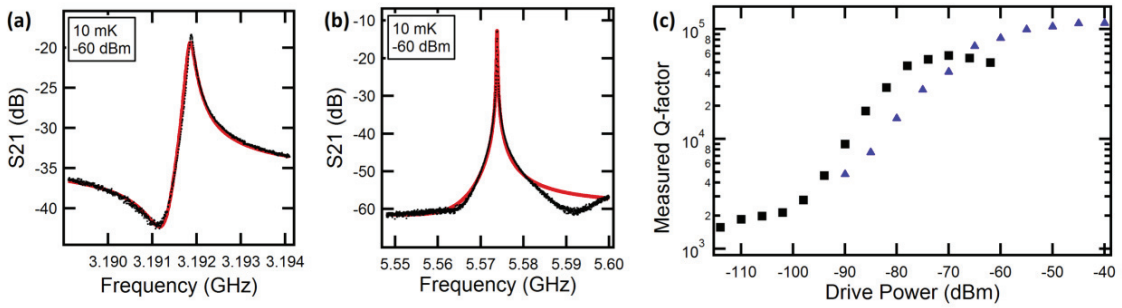


Figure 4: Nb coplanar resonators on MgO. (a) A typical asymmetric line-shape resonance that results from non-resonant parasitic coupling between input and output ports. (b) A Lorentzian line-shape produced by embedding the resonator in a low parasitic EM environment. (c) $Q$-factor measurements comparing the effect of parasitic environments. The suppression of $Q$ at low powers is due to two-level charge traps in the surrounding dielectric [6-8].

Finally, we compare $Q$-factors for devices embedded in low parasitic environments to those that exhibit asymmetric line-shapes. In both cases we find a strong dependence of $Q$-factor on input power to

the resonator. At low powers, recent work has highlighted the deleterious effect of microwave photons in the resonator coupling to two-level charge traps in the surrounding dielectric [6-8]. These trap states become unsaturated only at low powers and temperatures, and degrade the resonator performance in the low photon limit. $Q$-factors are extracted from fits to the resonance line-shape as described above and shown in Fig. 4(c) as a function of input power for a temperature of 10 mK. Blue triangles are values of $Q_M$ extracted from resonances similar to that shown in Fig. 4(a). Conversely the black squares are values obtained from a device exhibiting a resonance with a Lorentzian line-shape and corresponding low parasitic environment. At the highest powers studied here, our resonators also demonstrate non-linear effects as described by Abdo *et al* [14] and references therein.

## 4. Conclusions

Low power microwave transmission measurements of Nb coplanar resonators at milli-Kelvin temperatures were measured in two different electromagnetic environments. Small details such as the number of bond wires and abrupt changes in the geometry of interconnects can yield non-Lorentzian line-shapes and resonances that are shifted down in frequency from their expected value. We have measured $Q$-factors in excess of $10^5$ together with Lorentzian line-shape resonances using moderate power levels and environments optimized for low parasitic coupling. At low powers the $Q$-factor decreased steadily by nearly two orders of magnitude. These effects, reported elsewhere, have been attributed to the presence of two-level charge traps in either the dielectric or the interface between the superconductor and the dielectric substrate.

## Acknowledgements

We acknowledge support from the Australian Research Council, Centre of Excellence Scheme (CE110001013), CSIRO OCE Postgraduate Program, and thank J. I. Colless for technical assistance.

## References

[1] Siddiqi I, et al., Phys. Rev. Lett. 93, 207002 (2004).
[2] Tholen EA, Ergul A, Doherty EM, Weber FM, Gregis F, Haviland DB, http://arxiv.org/abs/cond-mat/0702280 (2007).
[3] Day PK, LeDuc HG, Mazin BA, Vayonakis A, Zmuidzinas J, Nature 425, 817-821 (2003).
[4] Wallraff A et. al., Nature 451, 162-167 (2004).
[5] DiCarlo L et. al., Nature 460, 240-244 (2009).
[6] O'Connell et. al., Appl. Phys. Lett., 92, 112903 (2008).
[7] Macha P et. al., Appl. Phys. Lett., 96, 062503 (2010).
[8] Sage J et. al., J. Appl. Phys., 109, 063915 (2011).
[9] Gevorgian S et. al., IEEE Trans. Microwave Theory, 43, 4 (1995).
[10] Pozar M, *Microwave Engineering*, J. Wiley (2005).
[11] Gao J et. al., Appl. Phys. Lett., 92, 152505 (2008).
[12] Wang H et. al., Appl. Phys. Lett., 95, 233508 (2009).
[13] Inomata K, Yamamoto T, Watanabe M, Matsuba K and Tsai JS, J. Vac. Sci. Technol. B 27, 2286 (2009).
[14] Abdo B, Segev E, Shtempluck O and Buks E, Phys. Rev. B, 73, 134513 (2006).